Title

Magnetically-responsive silica—gold nanobowls for targeted delivery and SERS-based sensing

Journal

Nanoscale, 8(23)

ISSN

2040-3364

Authors

Mo, Alexander H

Landon, Preston B

Gomez, Karla Santacruz

et al.

Publication Date

2016-06-09

DOI

10.1039/c6nr02445a

Peer reviewed

Published in final edited form as:

Nanoscale. 2016 June 09; 8(23): 11840–11850. doi:10.1039/c6nr02445a.

Magnetically-responsive Silica-gold Nanobowls for targeted delivery and SERS-based sensing

Alexander H. Mo[#1], **Preston B. Landon**[#†,2,3], **Karla Santacruz Gomez**[#3,5], **Heemin Kang**[1,2], **Joon Lee**[1], **Chen Zhang**[4], **Woraphong Janetanakit**[4], **Vrinda Sant**[2], **Tianyu Lu**[2], **David A. Colburn**[2], **Siddhartha Akkiraju**[4], **Samuel Dossou**[4], **Yue Cao**[2], **Kuo-Fen Lee**[6], **Shyni Varghese**[1,2,4], **Gennadi Glinsky**[3], and **Ratnesh Lal**[†,1,2,3]

[1]Materials Science and Engineering Program, La Jolla, CA 92037

[2]Dept. of Bioengineering, La Jolla, CA 92037

[3]Dept. of Mechanical and Aerospace Engineering & Institute of Engineering in Medicine,

[4]Dept. of Nanoengineering, University of California, San Diego, La Jolla, CA 92093.

[5]Departamento de Física, Universidad de Sonora, Hermosillo, Sonora, México, La Jolla, CA 92037

[6]Salk Institute for Biological Studies, La Jolla, CA 92037.

[#] These authors contributed equally to this work.

Abstract

Composite colloidal structures with multi-functional properties have wide applications in targeted delivery of therapeutics and imaging contrast molecules and high-throughput molecular bio-sensing. We have constructed a multifunctional composite magnetic nanobowl using bottom-up approach on an asymmetric silica/polystyrene Janus template consisting of a silica shell around a partially exposed polystyrene core. The nanobowl consists of a silica bowl and a gold exterior shell with iron oxide magnetic nanoparticles sandwiched between the silica and gold shells. Nanobowls were characterized by electron microscopy, atomic force microscopy, magnetometry, vis-NIR and FTIR spectroscopy. Magnetically vectored transport of these nanobowls was ascertained by time-lapsed imaging of their flow in fluid through a porous hydrogel under a defined magnetic field. These magnetically-responsive nanobowls show distinct surface enhanced Raman spectroscopy (SERS) imaging capability. PEGylated magnetically-responsive nanobowls show size-dependent cellular uptake *in-vitro*.

Visual Abstract

[†]**Corresponding Author:** Correspondence and requests for materials should be addressed to P.L (plandon@ucsd.edu) or R.L. (rlal@ucsd.edu), Tel +1 (858) 822-0384. Fax: +1 (858) 534-5722.

Contributions:

AM, PL, KSG, HK, KL, SV, KL, GG, RL, designed the experiments. AM, KSG, JL, DC, SA, SD, VS, TL, YC performed experiments. AM, PL, KSG, HK, analyzed the data. AM, PL, KSG, HK, JW, CZ, SV, GG, RL, wrote the paper.

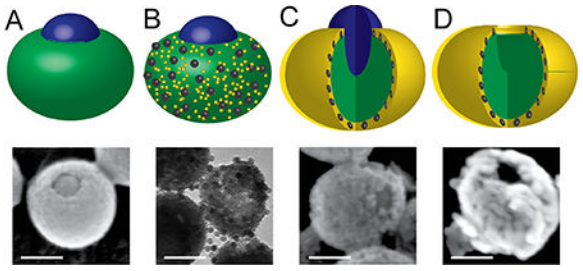

Keywords

gold shell; nanobowl; magnetic shell; SERS; iron oxide; controlled delivery

Introduction:

The ability to create colloidal structures with control over their size, geometrical architecture, material composition, and surface chemical functionalities are of immense interest. Such structures have potential applications in photonic[1], therapeutic drug delivery[2], and functional devices[3]. Composite colloids are of interest because two or more different materials are co-localized onto the same particle and their properties can be used in a complementary or synergistic fashion[4–6]. Composite colloidal structures have been synthesized using various physical[7–13] and chemical[14–19] methods. Composite colloids consisting of silica and different polymers are currently of great interest, because they can be readily synthesized[15, 20–23], consist of relatively inert materials, and are well suited as templates for the bottom-up fabrication of more intricate architecture such as core-shell nanostructures.

The bottom-up approach has been used to create a three layer silica-iron oxide-gold magnetic bowls by attaching magnetite iron oxide and gold nanoparticles to a silica core, followed by growth of gold shell over the silica[24, 25]. Also, hierarchical colloidal templates with a pollen-like shape have been used to create silica whiffle balls[26] and gold-silica golf balls[27]. Colloidal templates were created by electrostatic absorbance of smaller spheres (satellites) to a larger spherical core[26–31] and then the desired materials were selectively grown on the core of these templates. Also, asymmetric silica/polystyrene colloids have been synthesized that contains a polystyrene shell around a partially exposed silica core[16, 20, 32] or a silica shell around a partially exposed polystyrene core[21, 33, 34].

In the present study, we have used an emulsion-free method[35] to create a multifunctional gold magnetic nanobowl (AuMN). Starting with a template of silica with partially exposed polystyrene core, we added magnetic iron oxide nanoparticles and gold on top of the template to create a composite nanobowl with a gold exterior, a silica bowl interior, and iron oxide particles sandwiched in the middle. Nanobowl morphology and functional properties were evaluated by electron microscopy, AFM, magnetometry, and spectroscopy (vis-NIR, FTIR, Raman). Using a defined magnetic field, the transport of AuMN through a porous hydrogel was monitored at different time points. The biosensing and drug delivery potential of the nanobowls was evaluated through surface-enhanced Raman scattering (SERS)

detection of rhodamine B (Rho B) and 4-mercaptobenzoic acid (4-MBA) and size-dependent cellular uptake of nanobowls *in vitro*.

Results and discussion

Characterization of Nanobowl Synthesis:

Gold shell magnetic nanobowls (AuMNs) were created by using a multistep process summarized in Fig. 1. The process started with the synthesis of a silica/polystyrene Janus template using Stöber's method for silica particle formation modified with the addition of carboxylate polystyrene nanoparticles[35]. The silica in the templates was then functionalized with an amino alkoxysilane to render the silica surface positively charged. An outer shell was grown around the template in a two-step process. The template was first seeded with negatively charged iron oxide (IONP) and gold (AuNP) nanoparticles. Then a gold shell was grown by reducing seeded templates in a gold chloride solution. The gold surface was modified with polyethylene glycol to keep the particles well-dispersed. Finally, the gold-covered templates were turned into magnetically-responsive bowls by dissolving the exposed polystyrene in organic solvent.

In order to confirm the effectiveness of every step in the bowl synthesis process, changes in morphology at each step was visualized by electron microscopy imaging. The first step consisted of an one-pot reaction to form negatively-charged (−31.06 ± 2.39 mV) silica/polystyrene Janus templates (Fig. 2A). Modification of the Janus templates by an (3-aminoethylamino)propyl-trimethoxysilane (AEAPTMS) resulted in a positive surface charge as measured by zeta potential (+14.58 ± 2.17 mV). This allowed for the electrostatic attachment of negatively-charged 15 nm-sized IONP (−34.09 ± 3.31 mV) and gold-amine bonding by 3–5 nm-sized AuNP. IONPs were modified by the manufacturer (Ocean Nano, see Experimental for more details) with a strong negative surface charge. AuNPs were synthesized from the reduction of chloroauric acid ($HAuCl_4$) with tetrakis(hydroxymethyl)phosphonium chloride (THPC) in aqueous sodium hydroxide solution (pH >10). THPC both reduces the gold salt into small gold nanoparticles and serve as a neutral stabilizing agent (zeta potential, 1.21 ±1.62 mV). TEM images of well-washed IONP-AuNP coated templates show dense surface coverage of both the larger IONPs and the smaller AuNPs (Fig. 2B).

A combination of nanoparticle attachment order and pH played a critical role in attaining dispersed and densely attached templates. In order for the seeded templates to remain dispersed in solution, a rapid reversal of charge is required when using electrostatic assembly methods. Amine modified templates would often aggregate when solely in the presence of IONPs. Manufacturer supplied IONPs were at a sub-saturation concentration and thus neutralized the surface change (zeta potential typically, −10 to +10 mV) rather than completely reversing it. We reasoned that it was necessary to perform seeding with both IONP and gold at the same time, because the gold seeding concentration was sufficiently high to reverse the surface charge and stabilize the seeded templates. By adjusting the ratio of IONPs and Janus templates, the amount of IONPs on the Janus template can be further increased if needed.

Another important factor in our nanobowl synthesis was pH, because the gold seeding solution was synthesized in basic pH condition and remained at highly basic (pH>9). At such high pH values, aminated templates were generally neutral due to deprotonation of the majority of amines on the silica surface. Addition of IONPs into the seeding solution did not lower the pH significantly and attempts to seed in these conditions resulted in heavy agglomeration. Adjustment of the seeding solution to pH 7–8 with the addition of small amounts of 10 mM HCl to the IONP/gold solution resulted in non-agglomerated templates and successful seeding of both IONP and gold as evident in TEM image (Fig. 2B). In addition colloidal stability is further confirmed from zeta potential measurements showing highly negatively charged IONP-AuNP coated template (−30.45 ± 3.31 mV).

A complete shell was formed by suspending the IONP-AuNP coated templates in a $HAuCl_4$ plating solution and reducing the gold onto the templates (Fig. 2C). After formation of the gold shell, the gold-plated Janus template was suspended in thiolated polyethylene glycol (PEG) solution for 24 hours and then transferred to a solution of THF for another 24 hr to dissolve polystyrene (Fig. 2D). The composite magnetically-responsive nanobowls are a deep teal color when suspended in solution (Fig. 2E) and were magnetically attracted to the side wall of the container (Fig. 2F).

Various characterization modalities were used to confirm the completion of different steps of the synthesis process. First, after the Janus templates were formed, the surface of the Janus templates was modified with AEAPTMS and confirmed by FTIR analysis (Fig. 3). The FTIR spectrum showed peaks that correspond to primary amines at 1500 and 3600 cm^{-1}. In addition, the siloxane and silylhydride bonds were seen more prominently at 1100 and 2100 cm^{-1}, respectively. Second The absorbance measurements of the gold nanobowls showed the formation of absorbance peak at 840 nm, indicative of a gold shell around a silica core[36] (Fig. 4A). In addition, the magnetic hysteresis of the particles was measured with a vibrating sample magnetometer and the particles were found to be slightly ferromagnetic (Fig. 4B). The saturating magnetization for the magnetic gold shell nanobowls was between 0.4–0.6 emu/g. The 15 nm IONPs were usually superparamagnetic at the 15 nm size, but in this particular case, the composite particles appeared to have retained some ferromagnetic character with a noticeable hysteresis. This is attributable to the measurement being performed on a dry powder[36]. Third, the Vis-NIR absorbance measurements of the gold nanobowls showed the formation of absorbance peak at 840 nm, indicative of a gold shell around a silica core[37] (Fig. 4B). Spectrums recorded for gold seeding solution showed a characteristic absorbance peak around 550 nm. This peak started to shift as it was absorbed onto the silica surface of the Janus templates. Finally the peak around 840 nm around both gold shell covered templates and PEG-AuMN has not changed. This indicates the gold shell has not been adversely affected by the presence of the PEG.

Wide-field SEM images, AFM, and DLS of the gold-plated Janus templates and nanobowls showed the monodispersity of the nanobowls (Fig. 5 and S1). The PEGylated gold plated templates showed individual particles formed a complete gold shell over the external silica surface (Fig. 5A). After removal of polystyrene by THF, dark holes in the gold shells appeared indicating removal of the polystyrene and no noticeable changes in dispersity were noted (Fig. 5B). DLS particle sizing before THF revealed two peaks at 266 nm and 669 nm

of the sample (Fig. 5C, green). Particle sizing after THF (Fig. 5C, red) showed a slight increase in diameter of the two peaks (279 nm, 765 nm) when compared to pre-THF measurement (Fig. 5C, green). The 266 and 279 nm peaks in both curves of Fig. 5C represented approximately 80% of the population and matched well with the diameter of to individual nanobowls in SEM images (Fig. 5A–B). The larger diameter peaks corresponded to some aggregates that were also visible in SEM images of pre-THF gold Janus templates (Fig. 5A) and post-THF nanobowls (Fig. 5B). A paired two-sample t-test on the two DLS curves showed that the two populations are not statistically different ($p<0.05$) from each other.

Magnetic Transport

We then verified the ability of the nanobowls for directed transport under a magnetic field by acquiring time course images of their passage through porous hydrogels in PBS under a permanent magnetic field over a span of 52 hr (Fig. 6). A cylindrically shaped gelatin-methacrylate-*co*-N-acryloyl 6-aminocaproic acid hydrogel (Fig S2) with approximately 50 micron-sized pores was laid on its side in a glass vial containing PEGylated nanobowls in PBS and a strong rare earth magnet at one end of the glass vial. PEGylated magnetically-responsive nanobowls over the time course were attracted toward the magnet and the infiltration of the particles in the hydrogel was visualized as teal tint within a previously clear gel. The gel became progressively more teal colored over the time (Fig. 6A–E). On closer examination, a front of particles was seen infiltrating the porous hydrogel from the right to the left side (toward the magnet) and becoming more diffuse in the gel as time progressed (Fig. 6F–H). This suggests a potential use of the nanobowls for magnetically controlled delivery through soft tissues. An arrow in Fig. 6 F–H indicates the direction and movement of nanobowls towards the left side of each image.

AuMN as SERS plaform

We examined the application of gold/silica nanobowls as SERS platform for the detection of specific molecules. Rhodamine B (Rho B) and the most common non-resonant analyte, 4-mercaptobenzoic acid (4-MBA) were used as Raman-reporters in order to evaluate SERS capabilities of the AuMNs. The Raman enhancement effect can be maximized when the frequency of the excitation laser approach the resonance frequency of the localized surface plasmon in metallic nanoparticles[38]. The magnitude of the improvement of the Raman signal was estimated throughout the enhancement factor (EF), which was calculated based on the following equation[39]:

$$EF = (I_{SERS}/N_{surf}/(I_{RS}/N_{vol})$$

where I_{SERS} and N_{surf} are the intensity of the Raman signal and the number of the Raman reporter molecule in the scattering volume for the SERS sample respectively. N_{vol} and I_{RS} represent the average number of molecules in the scattering volume and the intensity of the Raman signal respectively for the probe molecule without AuMNs.

Fig 7 shows the Raman spectra of both Rho B and 4-MBA used as probe molecules, in the presence and in absence of the AuMNs. The presence of the nanobowls significantly affects the Raman signal of the Rho B with no shift of the peaks position of the normal sample. Figure 7A shows that the SERS phenomenon is dominated by at least six peaks located at 621, 1201, 1277, 1358, 1505 and 1648 cm^{-1}, which corresponds well to those reported for the Rho B in previous work[40, 41]. The EFs were found to be around 10^5-10^6 (Table S1), which is similar to the published work with other nanoparticles[42]. In order to better evaluate the SERS property of these AuMNs, we used a non-resonant sample as probe molecule. Raman spectra were obtained in similar conditions for 4-MBA molecules in the presence or in absence of AuMNs. A number of peaks appear in SERS measurements compared with the 4-MBA alone, which were previously reported for 4-MBA in other SERS nanoparticles[43] Five peaks located at 805, 1102, 1138, 1291 and 1597 cm^{-1} were used to estimate the EF. The EF was estimated to be ~10^5 (Table S2). These results reveal the good SERS capability of these AuMNs, which make this nanostructure suitable for a very sensitive analytical sensing.

In vitro incubation of AuMN

Before incubation with cells, PEG-AuMNs were modified with a FTIC-silane conjugate. In order to provide easy visualization under fluorescence microscopy (Fig S3), FITC was reacted with APTES in anhydrous ethanol in order to create FITC-silane conjugate. Then FITC-silane was added to a THF solution containing AuMN in order to react. Fluorescence microscopy was used to confirm FITC-silane attachment to the interior of the bowl. Figure S2 shows FITC-PEG-AuMN particles on a glass slide at different concentrations.

FITC-PEG-AuMNs uptake and their cellular response were examined in WPMY-1 normal human prostate and LNCaP cancerous human prostate cell lines. The AuMN were introduced at different initial concentrations and incubated with the cells for varying lengths of time up to 24 hours. Overall the cells exhibited a dose dependent response to AuMN particles. At the lower concentration measured (0.001 mg/mL) no cellular toxicity is observed in either cell line even after 24 hr. (Fig. 8 A and C). At the highest concentration measured (0.1 mg/mL), approximately 60% of cells were still alive after 2 hr in both cell lines. After 24 hours, only 50% of cells were alive in the WPMY-1 cell line and about 30% were still alive in LNCaP cells group. Merged phase contrast-fluorescent images show cell uptake in WPMY-1 (Fig. 8B) and LNCaP (Fig 8D) cells as well.

In vitro cellular uptake of AuMNs was also evaluated by atomic force microscopy (AFM)[44, 45]. For the *in vitro* uptake analysis, WPMY-1 cells were incubated with PEGylated- gold nanobowls for 2 hours. PEG is usually used to reduce the macrophage uptake and prolong nanoparticles circulation half-life[46]. Earlier studies suggested that PEGylation increased nanoparticle stability and improved their cellular biocompatibility[47, 48]. As seen in AFM images (Fig. 8E–H), after 2 hours of incubation, the magnetic nanobowls were distributed heterogeneously into the cytoplasm in a size-dependent manner. Larger nanobowls were located on the cell periphery (Fig. 8G, blue circles), whereas smaller nanobowls appeared to be endocytosed into the cytoplasm (Fig. 8G, black circles). These results are consistent with previous observations that endocytosis

of colloids is primarily related to size, shape and surface properties of nanostructure[49, 50]. AFM images of WPMY-1 cells treated with magnetic gold nanobowls show the presence of spots in the treated cells (Fig. 8H). The diameter of the nanobowls (denoted by spots in Fig. 8H) located inside the cells is 274±3 nm, similar to the size obtained from AFM of the magnetic gold nanobowls by themselves (Fig. S3) and the size distribution of magnetic gold nanobowls in DLS (Fig. 5). Typically, a total of 43 spherical nanoparticles per cell were observed. No significant changes in the normal morphology of the WPMY-1 cells or visible nanoparticles aggregation were observed after 2 hours of incubation of magnetic nanobowls in a 0.001 μg/ml dilution. The presence of larger (275 nm diameter) nanobowls in the cytoplasm suggests that even large nanobowls can eventually be endocytosed. In addition we have demonstrated previously that the Janus template diameter can be controlled[51] and correspondingly the nanobowls can also be controlled as well. The mechanism of such cellular uptake, though important is beyond the scope of this manuscript.

Although not studied in this work, nanobowls can be used as a drug delivery vehicle by putting a biocompatible cap on the bowl, including liposomes[52], chitosan[53], and PLGA[54]. For conditional and controlled release of the therapeutic agent from the bowl, such a cap could be released by specific interaction with nucleic acid molecules[50–53], enzymatic processes, or environmental triggers like temperature and pH. Existing delivery systems usually have pores or open surfaces that allow passive and/or continuous release of their loads (imaging contrast molecules or therapeutic agents)[44, 55]. Our nanobowls can be used for a magnetically-guided delivery and controlled on-demand release of imaging contrast molecules and therapeutic (theranostic) agents.

Conclusion

In conclusion, we have synthesized magnetic gold nanobowls using an asymmetric silica/polystyrene Janus template. The template was covered by small iron oxide nanoparticles coated with a gold shell. However, since gold only covered the silica and not the polystyrene, the symmetry of the shell is broken. This provides access to the interior of the bowl once the polystyrene is dissolved. Such a nanobowl has many advantages such as its interior volume for storage, differential functionalization with gold (exterior) and silica (interior) to allow simultaneous imaging in optical and near infra-red optical range, and magnetically guided targeted transport of the theranostic materials due to its embedded iron oxide nanoparticles. Present experimental evidence revealed a distinct SERS capability and size-dependent *in vitro* cellular uptake of our magnetically-guided nanobowls. These advantages make them an attractive candidate as a theranostic (therapeutics and diagnostics) nano carrier/vehicle. We believe that our gold nanobowls will have multiple robust and effective useful future applications for storing drug and imaging contrast molecules as depots for increase bio-availability and long term controlled release as well as for guided delivery to specific tissues and organs, including commonly inaccessible brain tissue, small organs such as pancreas and multi organs diseases such as cancer.

Experimental

Materials:

Carboxylate modified polystyrene (PS-COOH) spheres (100 nm 2.7% in water) were purchased from PolySciences. Tetrakis(hydroxymethyl) phosphonium chloride(THPC, 80% in water) sodium hydroxide(NaOH,10M), and chloroauric acid trihydrate ($HAuCl_4 \cdot 3H_2O$ 99.9%) were purchased from Aldrich. Potassium carbonate (K_2CO_3), formaldehyde (37%) and ammonium hydroxide (NH_3OH, 29.79%) were purchased from Fisher Scientific. Anhydrous Ethyl alcohol (EtOH) was purchased from JT Baker. (3-Aminoethylamino)propyl-trimethoxysilane (AEAPTMS), anhydrous isopropanol, tetrahydrofuran (THF), O-(2-Mercaptoethyl)-O′-methylpolyethylene glycol (10 kDa, mPEG-SH) was purchased from Sigma. Deionized (DI) water used in samples was produced using a Millipore Advantage A10 system with a resistance of 18.2 MΩ. Phosphate buffered saline (PBS, 1x) was purchased from Corning.

Janus template formation:

In a 250 mL glass vial with a magnetic stir bar, we added, in order, 7 mL DI water + 40 mL isopropanol alcohol + 13 mL of ammonium hydroxide. We then added 40 mM TEOS (550 μL) and 1 mL PS-COOH spheres at the same time while the solution stirring and allowed to stir for 2 hrs. The actual formation of the Janus template happened rather quickly; within the first 15–20 minutes of the reaction. The solution was then transferred to a centrifuge tube and centrifuged for 5 min @ 500 g to separate out agglomerated particles from lighter particles. The pellet was disposed of while the supernatant was transferred to a fresh centrifuge tube and centrifuged again at 3221 g for 15 minutes to settle the single particles. The supernatant was washed twice in 30 mL DI water and resuspended in 20 mL of anhydrous ethanol.

Preparation of gold seeds:

In 54 ml of water 50 μL of 10M sodium hydroxide was added and stirred well. In a separate container, 1 ml of water and 12 μL of 80% THPC were added to the original solution and the reaction was stirred for 5 min before 1.5 ml of chloroauric acid (10 mg/mL) was added. The solution was stirred for another 30 min at room temperature and incubated at 4°C for 24 hours before use.

Gold plating solution:

50 mg of K_2CO_3 was dissolved in 47 mL of DI water and stirred for 5 minutes. 3 mL of chloroauric acid (10 mg/mL) was then added to the stirring solution. The gold solution was initially light yellow and became clear after 30 min of stirring. Afterwards, the gold hydroxide solution was incubated for 24 hr at 4°C before use.

Janus template surface modification.

Asymmetric Janus templates were functionalized with amines by placing Janus templates into a solution containing 20 mL of anhydrous ethanol and 40 μL of AEAPTMS (final: 0.2 %v/v). The solution was stirred at 60ºC for 2 hrs. The amine functionalized Janus

templates were washed 3 times in ethanol and resuspended in 5 mL of anhydrous ethanol. The particles are the transferred to a glass vial and dried under vacuum under mild heating overnight.

Attachment of iron oxide and gold nanoparticles to Janus templates.

5 mg of dried amine modified Janus templates were weighed out and dispersed 1 mL of water with sonication as needed. 200 μL of 10 nm iron oxide solution was added to 1 mL of THPC-gold seed solution. The pH was adjusted to 8 by using sodium hydroxide or hydrochloric acid before adding the 1 mL of amine modified Janus templates into solution. The combined solution was allowed to tumble overnight, allowing proper time for attachment gold and iron oxide nanoparticles. The attached particles were then washed 3 times in water and a dark red pellet was redispersed in 2 mL of water.

Gold plating:

Gold and iron oxide seeded Janus templates (1 mg) were added into well-stirred solution of gold plating solution (5 mL), deionized water (4 mL) and 10 mM sodium citrate (1 mL). Then 26 μL of 37% formaldehyde was added to the solution and stirred for approximately 5 minutes. The solution proceeded from clear to pink to a greenish-blue during this time. The final solution had a dark green tint. Gold plated templates were then washed once and centrifuged at 2000g for 10 minutes before being resuspended in 1 mL of water.

PEGylation protocol:

50 mg of mPEG-SH (10 kDa) was dissolved in 1 mL of water and added to a 1 mL solution of gold shell Janus templates. The solution was allowed to tumble overnight before washing twice at 2000 g for 10 minutes.

Nanobowl Formation:

Nanobowls were formed by dissolving the exposed polystyrene in gold plated templates. The 2 mL of gold was centrifuged and re-suspended in 2 mL of ethanol before being transferred into a glass centrifuge vial containing 10 mL of THF. The solution was allowed to stir overnight before washing and re-suspension in 2 mL of water.

Nanobowl formation/FITC-silane attachment:

Freshly PEGylated particles were synthesized in a manner as described above. Fluorescein isothiocyanate (FITC, Sigma) and aminopropyltrimethoxysilane (APTES, Sigma) were suspended together in 1 mL of ethanol and tumbled together over night in the dark. Afterwards the FITC-APTES conjugate solution was added to the 4mL of THF and 1 mL of PEGylated gold-iron oxide-silica-polystyrene particle suspended in water. Again the magnetic gold nanobowls are formed while the FITC-APTES is attached to the bowl of the particle. The particles were then washed in water 3 times in 10 mL water and centrifuged at 2000 g for 5 minutes each time. The particles were then resuspended in 2 mL of water

Synthesis of gelatin-methacrylate-*co*-N-acryloyl 6-aminocaproic acid (GelMA-*co*-A6ACA) porous hydrogels:

Gelatin-methacrylate (GelMA) and N-acryloyl 6-aminocaproic acid (A6ACA) were synthesized as previously described [56, 57]. GelMA-*co*-A6ACA porous hydrogels were prepared by using polymethylmethacrylate (PMMA) porogen leaching method. Cylindrical polypropylene mold was filled with 65 mg of PMMA microbeads (Bangs Laboratories, diameter: 165 μm). 60 μl of a precursor solution containing 15% (w/v) GelMA and 9.25% (w/v) A6ACA as well as a photoinitiator of 0.3% (w/v) Irgacure 2959 was cast into the PMMA-packed mold and photopolymerized under 365 nm UV light for 10 min. The porous hydrogels were obtained by dissolving PMMA microspheres in acetone for 3 days. The porous hydrogels were equilibrated in PBS and cut into a cylindrical shape with diameter and thickness of 5 mm and 2 mm, respectively, prior to the introduction of magnetic nanobowls.

FTIR:

Fourier transform infra-red measurements were carried out with an Alpha series (Bruker) FTIR spectrometer equipped with a single reflection attenuated total reflectance module. Colloidal suspensions were dried under vacuum and the resulting sample was placed in the FTIR. 32 signals were acquired in transmittance mode and averaged to produce a spectrum.

SEM:

SEM samples were prepared by spreading out 20 μL of sample into four to five spots on an aluminum SEM post and allowed to air-dry. Images were taken on a FEI XL30 with an FEI Sirion column to enable higher resolution with an accelerating voltage of 15 kV. SEM imaging was carried out to examine a porous structure of the freeze-dried hydrogels. The pore diameter of the hydrogels in the dried state was estimated from 10 pores of each of three SEM images (n=30) using ImageJ. The data are shown as mean ± standard errors.

DLS:

Hydrodynamic size of the nanobowls was averaged over 5 measurements for each sample with a Particle size analyzer (Brookhaven Instrument Corp., Zetaplus/BI-PALS). Two different sets of samples were measured: samples before the removal of polystyrene from the template and samples after removal of Polystyrene from the template. The nanobowls were sonicated for at least five minutes to make sure that they were well dispersed in the solution. Then the samples were diluted by at least 100 fold in DI H_2O, in order to prevent the agglomeration of the nanobowls.

Zeta Potential Measurement:

Zeta Potential was measured with a Zeta potential analyzer (Brookhaven Instrument Corp., Zetaplus/BI-PALS) for the following five sets of samples: silica/polystyrene template, AEAPTEMS modified Janus template, IONP, AuNPs, and IONO-AuNO coated template. The samples were diluted 100 fold in DI H_2O and the Zeta potential of individual samples was measured over five 5 runs and then averaged. The averaged zeta potential for each samples are reported in the Results and Discussion section.

TEM:

Samples were prepared by placing a holey carbon coated TEM grid on a sheet of blotting paper. 20 μL of sample was added to the grid and allowed to sit for 15 min to allow the sample to adsorb. The sample was quickly dried using another sheet of blotting paper. The TEM grid was allowed to dry before imaging. The TEM grids were loaded into the sample holder of a JEOL 1200 EX II TEM operating at 60 kV and images were acquired using a Gatan Orius 600 digital camera.

Vibrating Sample Magnetometer:

The sample was dried in glass vial under vacuum and placed in a vibrating sample magnetometer (Quantum Design) to measure the magnetic behavior at 300 K.

SERS measurement:

Raman spectra were obtained using a Jobin Yvon/HORIBA LabRam Raman spectrometer integrated with a confocal microscope. Raman Spectra were collected in the range from 600 to 1800 cm^{-1} with an accumulation time of 30 seconds using a 633 nm diode laser.

AFM Nanoparticles characterization:

A multimode Nanoscope (Vecco Instruments) was used in tapping mode to characterize the AuMNs under ambient conditions, using a cantilever with a spring constant of 48 N/m. A clean mica substrate was coated with a drop of Poly-l-Lysine (0.01%) for 2 minutes and rinsed with ultrapure distilled water, and dried. 50 mg of nanobowls was deposited in the mica substrate during 15 minutes at room temperature. Samples were washed with ultrapure water and dried. AFM images were recorded in 50, 20 and 3 μm scan areas for the particles size distribution.

Fluorescent visualization of the in vitro uptake of magnetically-responsive nanobowls after incubation with human WPMY-1 and LNCaP cells:

WPMY-1, a human prostate cell line, and LNCaP, a human carcinoma line, were used to test cell viability upon exposure to FITC-PEG-AuMN for increasing amounts of time. WPMY-1 and LNCaP were obtained from the American Type Culture Collection (ATCC CRL-285). WPMY-1 and LNCaP cells were cultured using Dulbecco's Modified Eagle's Medium (DMEM, Gibco) containing 5% of fetal bovine serum (FBS, Gibco) at 37○C in humidified atmosphere of 5% of CO_2. Cells were grown in 60 mm petri dishes to reach a confluence of 70–80%. For imaging, WPMY-1 and LNCaP were treated with FITC conjugated, pegylated, AuMNs in a Phosphate-buffered saline (PBS, Corning) solution at different concentrations (0, 0.001, 0.01, 0.1 mg/mL). After different time intervals (0,2,4, 24 hr), cells were washed with PBS, further fixed using 0.4% glutaraldehyde (Sigma) for 5 minutes, and washed with PBST (PBS with 5% of Tween-20) solution three times. 3 ml of PBS was added afterwards. Additionally WPMY-1 and LNCaP cells were exposed to same concentrations of FITC conjugated, pegylated AuMNs (0, 0.001, 0.01, 0.1 mg/mL) and times (0, 2, 4, 24 h) were assayed for cell viability with the MTT assay (ThermoFisher). MTT absorbance measurements were made in triplicate to arrive at average cell viability.

AFM Visualization of the in vitro uptake of magnetically-responsive nanobowls after incubation with human WPMY-1 cells

WPMY-1 cells were growth and prepared as described for the fluorescence microscopy. Atomic force microscopy (AFM) images were obtained using a Bioscope AFM integrated with a Zeiss Axiovert 135TV inverted light microscope, using the Nanoscope3 software. Imaging of WPMY-1 treated and untreated cells was performed in PBS using the contact mode AFM. Cantilevers with nominal spring constant (k) of 0.02 N/m were utilized for imaging height and deflection modes. Images in scan area of 50 and 15 mm were recorded in 512 pixels format.

Supplementary Material

Refer to Web version on PubMed Central for supplementary material.

Acknowledgements

We would like to thank Professor Jan Talbot for access to the DLS instrument. We thank NANO3 staff for access to the SEM and related support. We thank Issac Liu and Professor Sungho Jin for access to the VSM. Also thanks to UCSD Electron Microscope Facility staff Timothy Meerloo and Ying Jones for access the TEM and related support. Thanks to Matthew Rozin for help with the UV-vis-IR spectrometer. Finally thanks to Professor Seth Cohen for access to the FTIR instrument. This work was funded by UCSD startup funds and NIH grants R01DA024871 and R01DA025296 to R.L. Post-doctoral Fellowship (237085) provided by Consejo Nacional de Ciencia y Tecnología (CONACyT) to K.S-G. In the supplemental, Additional SEM images of the hydrogel, AFM images of magnetically-responsive gold nanobowls, fluorescently tagged nanobowls, and Rhodamine b and 4-MBA SERS peaks for the gold nanobowls

References

1. McConnell MD, Kraeutler MJ, Yang S and Composto RJ, Nano Letters, 2010, 10, 603–609. [PubMed: 20063864]
2. Wang F, Pauletti GM, Wang J, Zhang J, Ewing RC, Wang Y and Shi D, Advanced Materials (Weinheim, Germany), 2013, 25, 3485–3489.
3. Wu Y, Wu Z, Lin X, He Q and Li J, ACS Nano, 2012, 6, 10910–10916. [PubMed: 23153409]
4. Walther A and Müller AHE, Chemical Reviews, 2013, 113, 5194–5261. [PubMed: 23557169]
5. Kaewsaneha C, Tangboriboonrat P, Polpanich D, Eissa M and Elaissari A, ACS Applied Materials & Interfaces, 2013, 5, 1857–1869. [PubMed: 23394306]
6. Binks BP, Current Opinion in Colloid & Interface Science, 2002, 7, 21–41.
7. Nisisako T, Torii T, Takahashi T and Takizawa Y, Advanced Materials (Weinheim, Germany), 2006, 18, 1152-+.
8. Kaufmann T, Gokmen MT, Wendeln C, Schneiders M, Rinnen S, Arlinghaus HF, Bon SAF, Du Prez FE and Ravoo BJ, Advanced Materials (Weinheim, Germany), 2011, 23, 79-+.
9. Maye MM, Nykypanchuk D, Cuisinier M, van der Lelie D and Gang O, Nature Materials, 2009, 8, 388–391. [PubMed: 19329992]
10. Walther A, André X, Drechsler M, Abetz V and Müller AHE, Journal of the American Chemical Society, 2007, 129, 6187–6198. [PubMed: 17441717]
11. Hong L, Jiang S and Granick S, Langmuir, 2006, 22, 9495–9499. [PubMed: 17073470]
12. Roh KH, Martin DC and Lahann J, Nature Materials, 2005, 4, 759–763. [PubMed: 16184172]
13. Lattuada M and Hatton TA, Journal of the American Chemical Society, 2007, 129, 12878–12889. [PubMed: 17910450]
14. Chen T, Chen G, Xing S, Wu T and Chen H, Chemistry of Materials, 2010, 22, 3826–3828.
15. Feyen M, Weidenthaler C, Schüth F and Lu A-H, Journal of the American Chemical Society, 2010, 132, 6791–6799. [PubMed: 20420374]

16. Ge X, Wang M, Yuan Q, Wang H and Ge X, Chemical Communications, 2009, DOI: 10.1039/b901094g, 2765–2767. [PubMed: 19532948]
17. Tanaka T, Okayama M, Minami H and Okubo M, Langmuir, 2010, 26, 11732–11736. [PubMed: 20507141]
18. Roh K-H, Martin DC and Lahann J, Journal of the American Chemical Society, 2006, 128, 6796–6797. [PubMed: 16719453]
19. Tang C, Zhang C, Liu J, Qu X, Li J and Yang Z, Macromolecules, 2010, 43, 5114–5120.
20. Meng Z, Xue C, Lu L, Yuan B, Yu X, Xi K and Jia X, Journal of Colloid and Interface Science, 2011, 356, 429–433. [PubMed: 21324470]
21. Wang Y, Xu H, Ma Y, Guo F, Wang F and Shi D, Langmuir, 2011, 27, 7207–7212. [PubMed: 21539320]
22. Chen QH, Li QQ and Lin JH, Mater. Chem. Phys, 2011, 128, 377–382.
23. Zhang J, Jin J and Zhao HY, Langmuir, 2009, 25, 6431–6437. [PubMed: 19466790]
24. Stoeva SI, Huo F, Lee J-S and Mirkin CA, Journal of the American Chemical Society, 2005, 127, 15362–15363. [PubMed: 16262387]
25. Kim J, Park S, Lee JE, Jin SM, Lee JH, Lee IS, Yang I, Kim J-S, Kim SK, Cho M-H and Hyeon T, Angewandte Chemie, 2006, 118, 7918–7922.
26. Ortac I, Simberg D, Yeh YS, Yang J, Messmer B, Trogler WC, Tsien RY and Esener S, Nano Letters, 2014, 14, 3023–3032. [PubMed: 24471767]
27. Landon PB, Mo AH, Zhang C, Emerson CD, Printz AD, Gomez AF, DeLaTorre CJ, Colburn DAM, Anzenberg P, Eliceiri M, O'Connell C and Lal R, ACS Applied Materials & Interfaces, 2014, 6, 9937–9941. [PubMed: 24937196]
28. Sadowska M, Adamczyk Z and Nattich-Rak M, Langmuir, 2014, 30, 692–699. [PubMed: 24383456]
29. Desert A, Chaduc I, Fouilloux S, Taveau J-C, Lambert O, Lansalot M, Bourgeat-Lami E, Thill A, Spalla O, Ravaine S and Duguet E, Polymer Chemistry, 2012, 3, 1130–1132.
30. Désert A, Hubert C, Fu Z, Moulet L, Majimel J, Barboteau P, Thill A, Lansalot M, Bourgeat-Lami E, Duguet E and Ravaine S, Angewandte Chemie International Edition, 2013, 52, 11068–11072. [PubMed: 24009068]
31. Perro A, Duguet E, Lambert O, Taveau J-C, Bourgeat-Lami E and Ravaine S, Angewandte Chemie International Edition, 2009, 48, 361–365. [PubMed: 19025744]
32. Tan LH, Xing S, Chen T, Chen G, Huang X, Zhang H and Chen H, ACS Nano, 2009, 3, 3469–3474. [PubMed: 19817393]
33. Wang Y, Wang F, Chen B, Xu H and Shi D, Chemical Communications, 2011, 47, 10350–10352. [PubMed: 21853175]
34. Guignard F and Lattuada M, Langmuir, 2015, 31, 4635–4643. [PubMed: 25843702]
35. Mo AH, Landon PB, Emerson CD, Zhang C, Anzenberg P, Akkiraju S and Lal R, Nanoscale, 2015, 7, 771–775. [PubMed: 25431230]
36. Zhang L, He R and Gu H-C, Applied Surface Science, 2006, 253, 2611–2617.
37. Pham T, Jackson JB, Halas NJ and Lee TR, Langmuir, 2002, 18, 4915–4920.
38. Haynes CL and Van Duyne RP, The Journal of Physical Chemistry B, 2003, 107, 7426–7433.
39. Le Ru EC, Blackie E, Meyer M and Etchegoin PG, The Journal of Physical Chemistry C, 2007, 111, 13794–13803.
40. Sun CH, Wang ML, Feng Q, Liu W and Xu CX, Russian Journal of Physical Chemistry A, 2014, 89, 291–296.
41. Lin S, Hasi W-L-J, Lin X, Han S.-q.-g.-w., Lou X-T, Yang F, Lin D-Y and Lu Z-W, Analytical Methods, 2015, 7, 5289–5294.
42. Kahraman M, Daggumati P, Kurtulus O, Seker E and Wachsmann-Hogiu S, Scientific Reports, 2013, 3, 3396. [PubMed: 24292236]
43. Jiang L, You T, Yin P, Shang Y, Zhang D, Guo L and Yang S, Nanoscale, 2013, 5, 2784–2789. [PubMed: 23435689]

44. Kong SD, Lee J, Ramachandran S, Eliceiri BP, Shubayev VI, Lal R and Jin S, Journal of Controlled Release, 2012, 164, 49–57. [PubMed: 23063548]
45. Ramachandran S, Quist AP, Kumar S and Lal R, Langmuir, 2006, 22, 8156–8162. [PubMed: 16952256]
46. Couvreur P and Vauthier C, Pharm Res, 2006, 23, 1417–1450. [PubMed: 16779701]
47. Arnida A. Malugin and Ghandehari H, Journal of applied toxicology : JAT, 2010, 30, 212–217. [PubMed: 19902477]
48. Oh E, Delehanty JB, Sapsford KE, Susumu K, Goswami R, Blanco-Canosa JB, Dawson PE, Granek J, Shoff M, Zhang Q, Goering PL, Huston A and Medintz IL, ACS Nano, 2011, 5, 6434–6448. [PubMed: 21774456]
49. Shukla R, Bansal V, Chaudhary M, Basu A, Bhonde RR and Sastry M, Langmuir, 2005, 21, 10644–10654. [PubMed: 16262332]
50. Iversen T-G, Skotland T and Sandvig K, Nano Today, 2011, 6, 176–185.
51. Landon PB, Mo AH, Printz AD, Emerson C, Zhang C, Janetanakit W, Colburn DA, Akkiraju S, Dossou S, Chong B, Glinsky G and Lal R, Langmuir, 2015, 31, 9148–9154. [PubMed: 26244597]
52. Pan J, Wan D and Gong J, Chemical Communications (Cambridge, United Kingdom), 2011, 47, 3442–3444.
53. Fu JK, Zhu YC and Zhao Y, J. Mat. Chem. B, 2014, 2, 3538–3548.
54. Xue JM and Shi M, Journal of Controlled Release, 2004, 98, 209–217. [PubMed: 15262413]
55. Kong SD, Zhang W, Lee JH, Brammer K, Lal R, Karin M and Jin S, Nano Letters, 2010, 10, 5088–5092. [PubMed: 21038917]

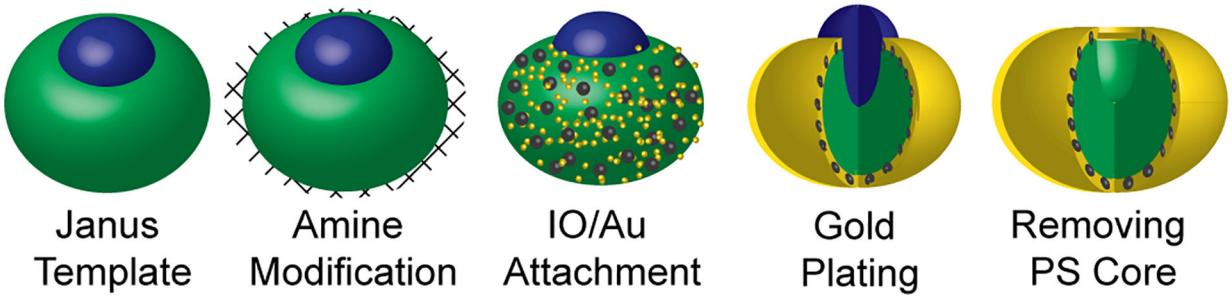

Fig. 1. Schematic of magnetic gold nanobowl formation.

A silica/polystyrene template is amine-modified and seeded with small gold and iron oxide nanoparticles. Later, a gold shell is grown in a plating solution, filling in the spaces between the gold nanoparticles. The magnetic gold bowl is finished by dissolving away the polystyrene in organic solvent.

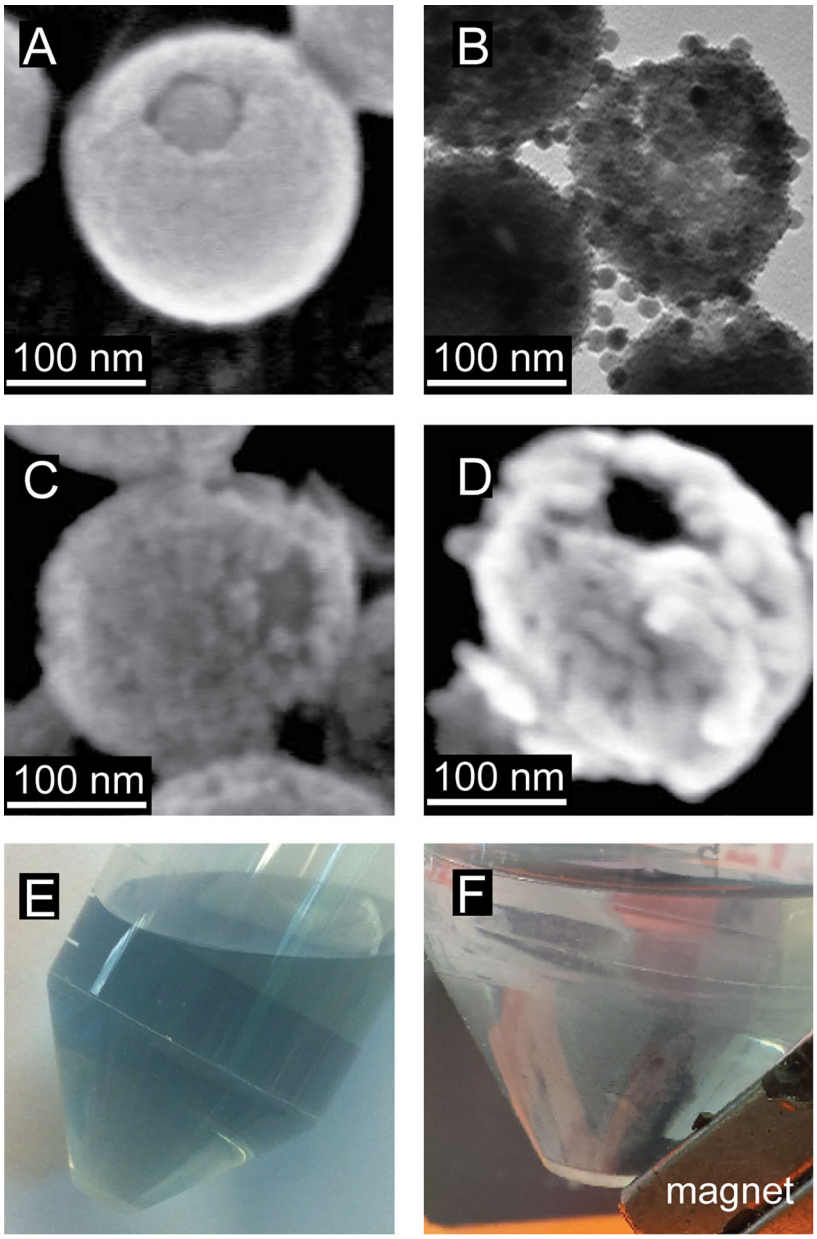

Fig. 2. Electron microscopy images of the synthesis process.

A) Janus template formation, **B)** gold and iron oxide nanoparticle attachment on silica, **C)** gold shell formation, and **D)** removal of polystyrene core. **E)** Gold plated particles in solution **F)** Magnetic gold/silica particles in solution attracted to magnet placed outside the container.

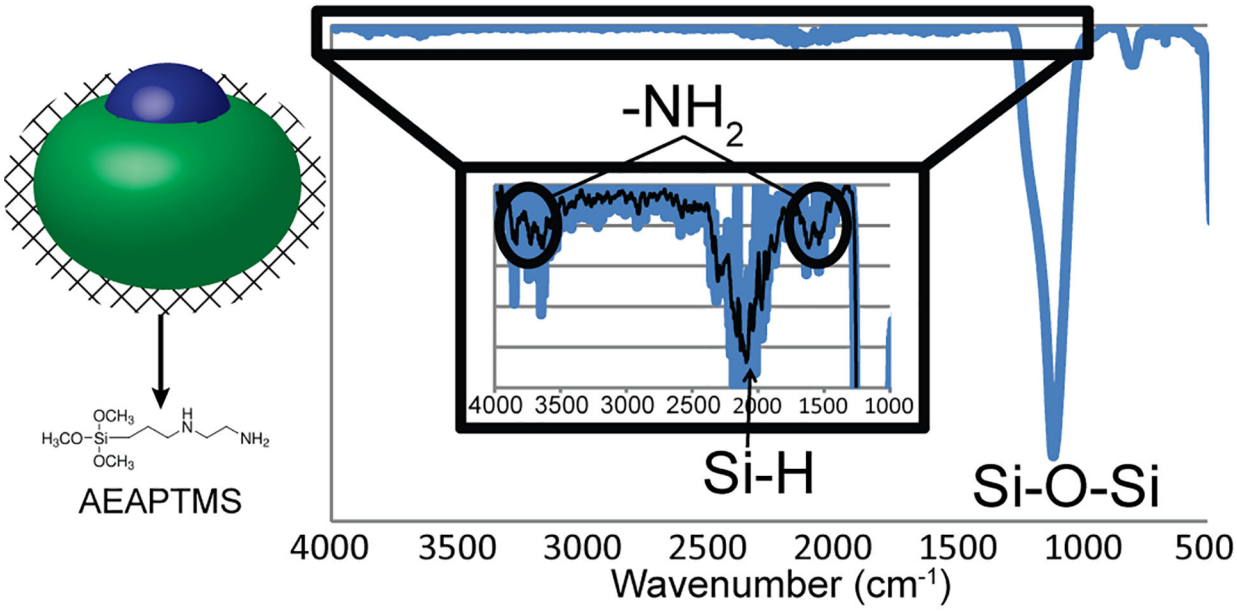

Figure 3. FTIR of amine-modified Janus template.

FTIR spectra shows the presence of peaks corresponding to amine (~1500 and 3600 cm^{-1}), siloxane bonds (1100 cm^{-1}), and silyl hydride bonds (~2100 cm^{-1}).

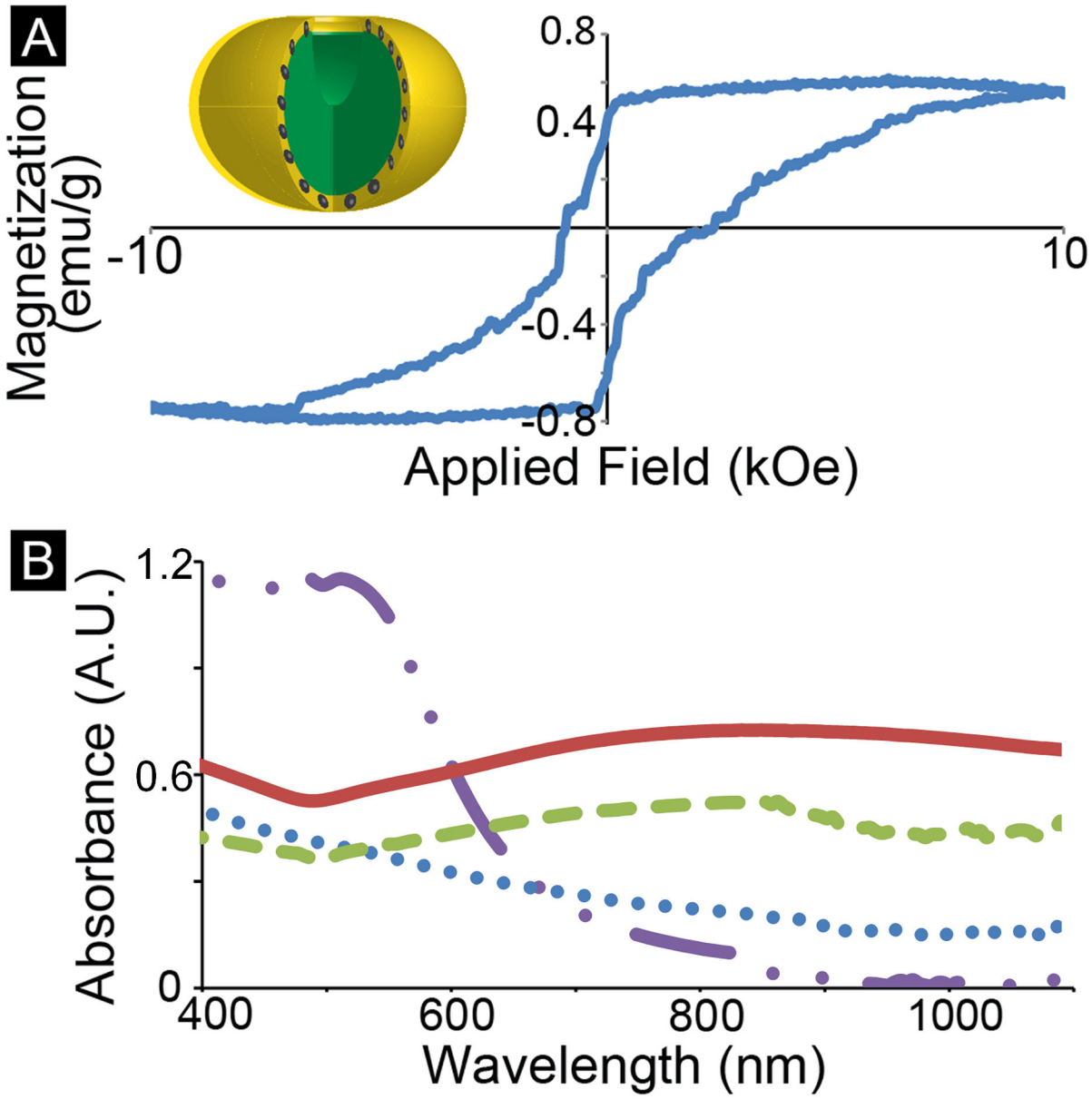

Fig. 4. Magnetic hysteresis and NIR spectrum of shell.

A) The magnetic hysteresis of the particles indicates that the composite particle retains some ferromagnetic character despite using 15 nm-sized ferromagnetic particles. **B)** NIR spectrum of different steps different times in synthesis process including gold nanoparticle seeds (double dot dash), gold seeded Janus templates (dotted blue line), gold shell nanobowls (dashed green line), gold shell nanobowls with PEG (solid red). The characteristic peak at around 550 nm for gold nanoparticles becomes a peak at the wavelength of 840 nm is indicative of successful gold shell formation. No change during the attachment of PEG indicates the PEG did not significantly disrupt the gold shells optical properties.

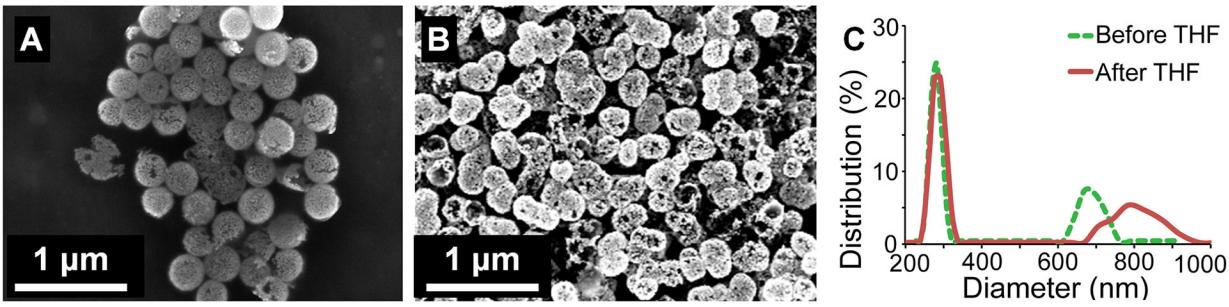

Fig. 5. Wide field images of PEGylated magnetic gold-silica.

A) Before and **B)** after removal of the polystyrene with accompanying **C**) DLS data for before (solid red, 266 nm, and 669 nm) and after removal of polystyrene (dotted green, 279 nm, 765 nm) in THF.

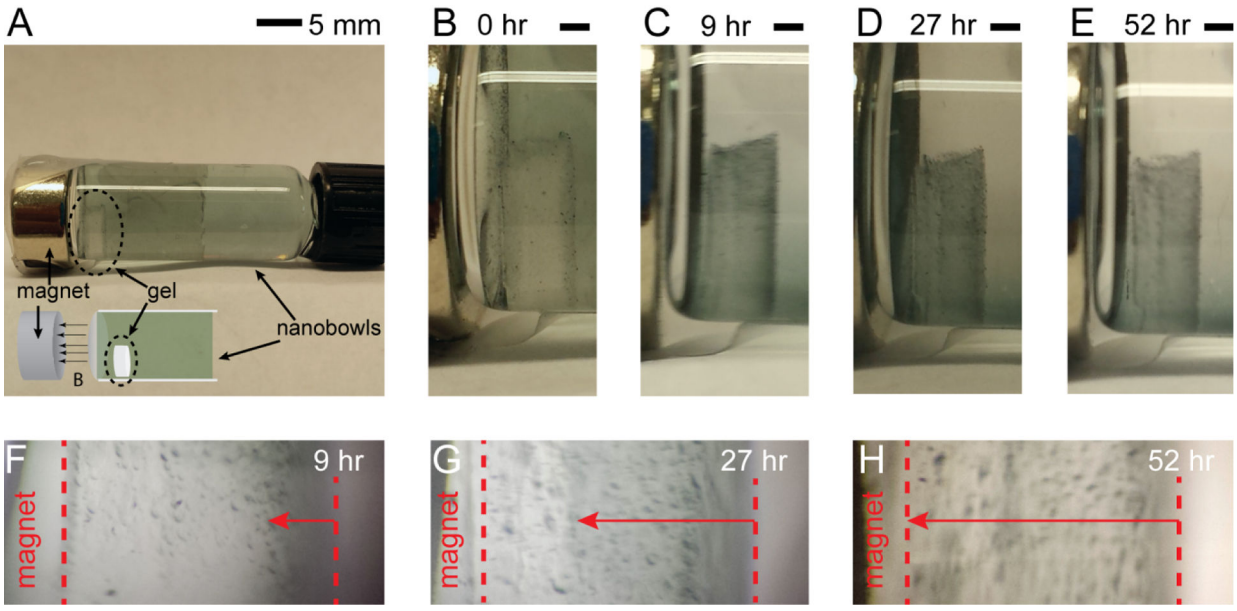

Fig. 6. Passage of gold magnetic nanobowls through hydrogel.

A) Experimental set-up for PEGylated magnetic nanobowls travelling through a GelMA-*co*-A6ACA porous hydrogel toward an ND-Fe-B magnet on the left. **B-E)** as time elapses, the gel becomes noticeably more teal colored on the right as the nanobowls infiltrate gel, travel into the gel and exit on the left. **F-H)** Under higher optical magnification, the movement of nanobowls can be observed through the gel at 9, 27, and 52 hr as indicated by the lengthening arrows. Gel boundaries are denoted by red dotted lines. **F)** At 9 hours, a teal colored front builds up on the right, **G**) at 27 hours, the particles move to the left and become more diffuse about two-thirds of the way through the gel, **H**) and at 52 hr, some nanobowls remain in the gel while most have already passed through the gel. Scale for **B-E** is 1 mm and for images **F-H**, the distance between the dotted lines is 2 mm.

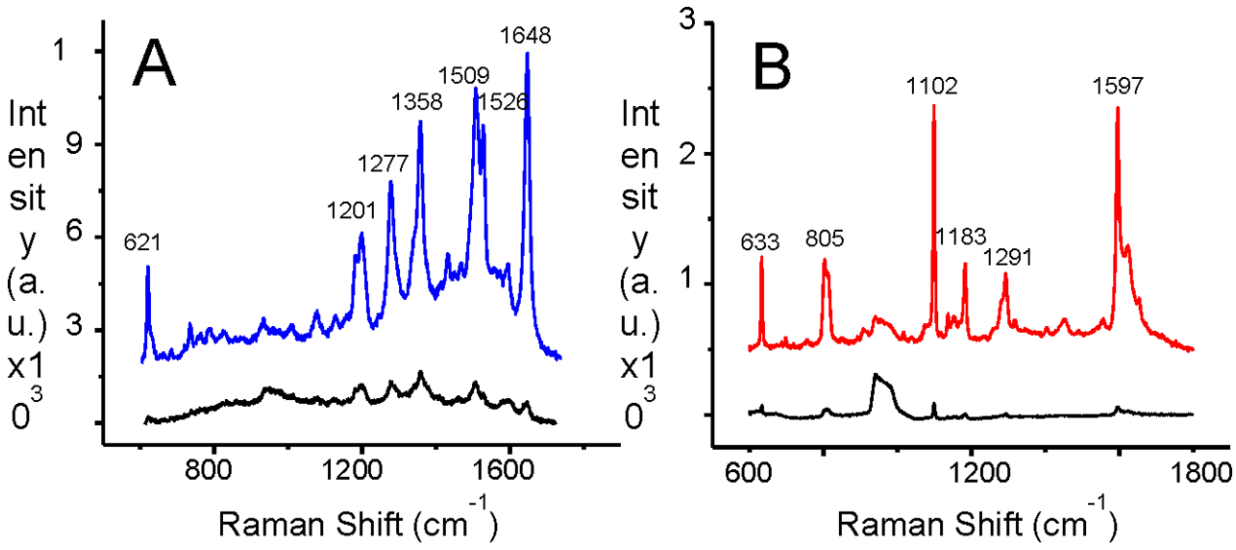

Fig. 7.

A) SERS spectra of 1×10^{-6} M Rho B on gold/silica nanobowls (top) and normal Raman spectrum of the Rho B (0.01 M) (bottom). **B)** SERS spectra of 4-MBA ($x10^{-5}$ M) (top) and normal Raman spectra of 4-MBA (0.3 M) (bottom). The numbers corresponds to the enhanced peaks.

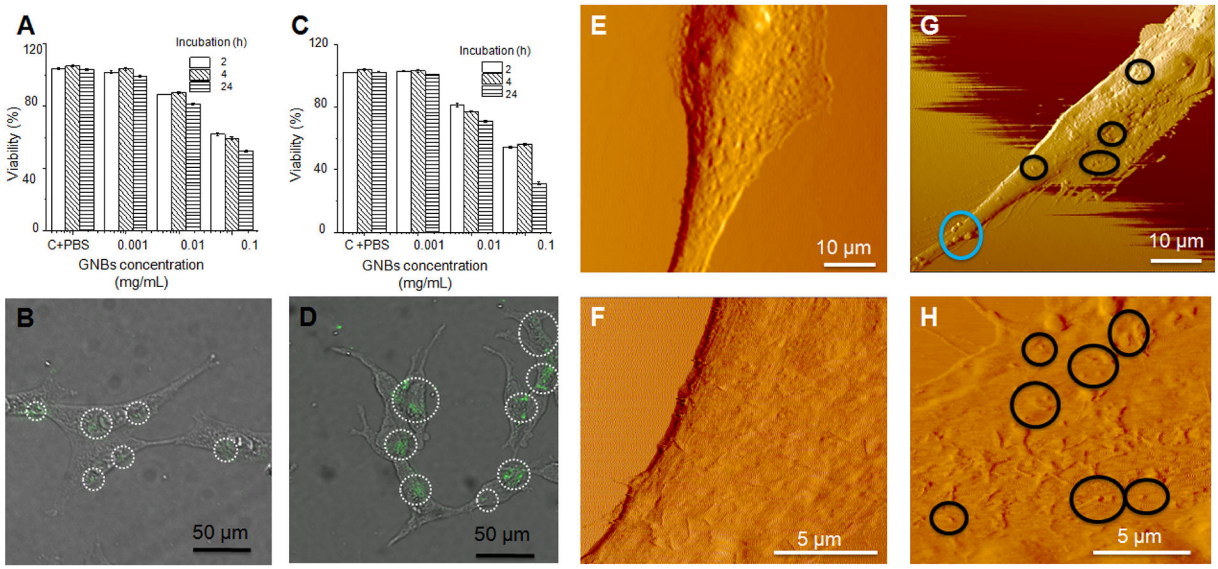

Fig 8.

In vitro uptake of PEG-AuMN. Relative cell viability for **A)**WPMY-1 after 2, 4 and 24 hours of incubation with AuMNs using the MTT assay. **B)** WPMY-1 fluorescence microscopy AuMNs uptake by after 4 hours of incubation. **C)** LNCaP MTT assay D) LNCaP fluorescence microscopy AuMN uptake after 4 hours of incubation. **B** and **D** are bright-field and fluorescence image merge. The fluorescence was obtained using the FITC filter l ex = 482±17nm and l em = 536±20 nm. WPMY-1 cell morphology were also imaged by AFM contact mode in PBS. Control with can areas of **E)** 50 µm and **F)** 15 µm as well as after the uptake of AuMNs scan areas of **G)** 50 µm and **H)** 15 µm. The smallest size nanoparticles (274 ± 3 nm) are located inside the cell (black circles), whereas larger nanoparticles did not enter the cells or remain in the periphery (blue circle).